

# Q-FIBRA: FEATURE AND INTENSITY BASED REGISTRATION WITH LARGE DEFORMATIONS VIA QUASI-CONFORMAL MAPS

KA CHUN LAM AND LOK MING LUI

**Abstract.** Registration, which aims to find an optimal one-to-one correspondence between different data, is an important problem in various fields. This problem is especially challenging when large deformations occur. In this paper, we present a novel algorithm to obtain diffeomorphic image or surface registrations with large deformations via quasi-conformal maps. The basic idea is to minimize an energy functional involving a Beltrami coefficient term, which measures the distortion of the quasi-conformal map. The Beltrami coefficient effectively controls the bijectivity and smoothness of the registration. Using the proposed algorithm, landmark-matching diffeomorphic (1-1 and onto) registrations between images or surfaces can be effectively obtained, even with a large deformation or large number of landmark constraints. The proposed algorithm can also be extended to a hybrid registration model, called *Q-Fibra*, which combines landmark and intensity (such as image intensity or surface curvature) information to obtain a more accurate registration. Experiments have been carried out on both synthetic and real data. Results demonstrate the efficacy of the proposed algorithm to obtain diffeomorphic registrations between images or surfaces.

**Key words.** Registration, landmark matching, intensity matching, quasi-conformal mapping, Beltrami coefficient, large deformations

**1. Introduction.** Registration is a process of finding the optimal one-to-one correspondence between different data, such as images or surfaces. Applications can be found in various fields, including computer graphics, computer visions and medical imaging. For example, in medical imaging, finding accurate 1-1 correspondence between medical data is crucial for statistical shape analysis of the anatomical structures. While in computer graphics, surface registration is needed for texture mapping.

Different registration approaches have been developed. Existing algorithms can mainly be divided into three categories, namely, 1. landmark-based registration, 2. intensity-based registration and 3. hybrid registration using both landmark and intensity information. Landmark-based registration computes a smooth 1-1 correspondence between corresponding data that matches important features. This kind of registration, with good feature alignment, is particularly crucial in medical imaging and computer graphics. For example, in computer graphics, landmark-based registration is used to obtain the constrained texture mapping. The main advantage of the landmark-based method is that larger deformations can be dealt with and intuitive user-interaction can be incorporated. Intensity-based registration aims to match corresponding data without feature landmarks. Registration is usually obtained by matching intensity functions, such as image intensity for image registration or surface curvature for surface geometric registration. The main advantage of the intensity-based registration is that more image information is taken into account and the delineation of feature landmarks is not required. However, it usually cannot cope with large geometric deformations. Recently, hybrid registration that combines landmark-based and intensity-based methods have gained increased attention. Hybrid approaches use both the landmark and intensity information to guide the registration. This type of approaches can usually obtain more accurate registration result, since the advantages of landmark-based and intensity-based registration can be combined. In this work, we will mainly focus on the landmark-based registration and the hybrid registration.

Most existing algorithms can compute registration accurately and efficiently when the deformation is small. However, the registration problem becomes challenging when large deformations occur. Bijectivity can be easily lost and overlaps can usually be

observed in the obtained registration. This causes inaccuracies in the registration. It is therefore necessary to develop an algorithm to obtain diffeomorphic registration with large deformations.

In this paper, we introduce a novel method to obtain diffeomorphic image or surface registrations via quasi-conformal maps, which can deal with large deformations. The key idea is to minimize an energy functional involving a Beltrami coefficient term, which measures the distortion of the quasi-conformal map. The Beltrami coefficient effectively controls the bijectivity and smoothness of the registration, even with very large deformations. By minimizing the energy functional, we obtain an optimal Beltrami coefficient associated to the desired registration, which is guaranteed to be bijective. Using the proposed algorithm, landmark-based diffeomorphic (1-1 and onto) registration between images or surfaces can be effectively obtained, even with a large deformation or a large number of landmark constraints. The proposed algorithm can also be combined with matching intensity (such as image intensity or surface curvature) to improve the accuracy of the registration. Numerical results show that the combination of landmark constraints with intensity matching can significantly improve the accuracy of the registration. To test the effectiveness of the proposed algorithm, experiments have been carried out on both synthetic and real data. Results show that the proposed algorithm can compute diffeomorphic registration between images or surfaces effectively and efficiently.

In summary, the contributions of this paper are three-folded. Firstly, we propose a variational method to search for an optimized Beltrami coefficient associated to a diffeomorphic quasi-conformal map with large deformations, which minimizes the local geometric distortion. Secondly, we apply the model to compute the landmark-based registration, which can deal with very large deformations and large amount of landmark constraints. Thirdly, we extend the landmark-based registration model to a hybrid registration model, called *Q-Fibra*, which combines both landmark and intensity information to obtain more accurate registration.

The rest of the paper is organized as follows. In Section 2, we review some previous works closely related to this paper. In Section 3, we describe some basic mathematical background related to our proposed model. In Section 4, our proposed model for diffeomorphic registration with large deformations is explained in details. We describe the numerical implementation of the proposed algorithm in Section 5. Experimental results are reported in Section 6. Finally, we conclude our paper in Section 7.

**2. Previous works.** In this section, we will review some previous works closely related to this paper.

Intensity-based image registration has been widely studied. A comprehensive survey on the existing intensity-based image registration can be found in [45]. One of the commonly used method is based on the variational approaches to minimize the intensity mismatching error. For example, Vercauteren et al. [36] proposed the diffeomorphic demons registration algorithm, which is a non-parametric diffeomorphic image registration algorithm based on Thirion’s demons algorithm[34]. The basic idea is to adapt the optimization procedure underlying the demons algorithm to a space of diffeomorphic transformations. The obtained registration is smooth and bijective. Glocker et al. [6][7][8] proposed the intensity-matching image registration algorithm using a Markov random field formulation. Several algorithms for surface registration that matches geometric quantities, such as curvatures, have also been proposed [3][32][25][41]. For example, Lyttelton et al. [32] proposed an algorithm for surface

parameterizations based on matching surface curvatures. Yeo et al. [41] proposed the spherical demons method, which adopted the diffeomorphic demons algorithm [36], to drive surfaces into correspondence based on the mean curvature and average convexity. Conformal surface registration, which minimizes angular distortions, has also been widely used to obtain a smooth 1-1 correspondence between surfaces [16, 14, 15, 39, 18, 20, 40, 44]. An advantage of conformal registrations is that they preserve local geometry well. Quasi-conformal surface registrations, which allows bounded amount of conformality distortion, have also been studied [29, 30, 43, 31]. For example, Lui et al. [30] proposed to compute quasi-conformal registration between hippocampal surfaces based on the holomorphic Beltrami flow method, which matches geometric quantities (such as curvatures) and minimizes the conformality distortion [29].

Landmark-based registration has also been widely studied and different algorithms have been proposed. Bookstein et al. [1] proposed to use a thin-plate spline regularization (or biharmonic regularization) to obtain a registration that matches landmarks as much as possible. Tosun et al. [35] proposed to combine iterative closest point registration, parametric relaxation and inverse stereographic projection to align cortical sulci across brain surfaces. These diffeomorphisms obtained can better match landmark features, although not perfectly. Wang et al. [38, 28, 26, 27] proposed to compute the optimized harmonic registrations of brain cortical surfaces by minimizing a compounded energy involving the landmark-mismatching term [38, 28]. The obtained registration is an optimized harmonic map that better aligns the landmarks. However, landmarks cannot be perfectly matched, and bijectivity cannot be guaranteed under large number of landmark constraints. Later, Lin et al. [24] propose a unified variational approach for registration of gene expression data to neuroanatomical mouse atlas in two dimensions that matches feature landmarks. Again, landmarks cannot be exactly matched. Inexact landmark-matching registrations are sometimes advantageous. In the case when landmark points/curves cannot be accurately delineated, this method is more tolerant of errors in labeling landmarks and gives better parameterization. In the situation when exact landmark matching is required, smooth vector field has been applied to obtain surface registration. Lui et al. [26, 27] proposed the use of vector fields to represent surface maps and reconstruct them through integral flow equations. They obtained shape-based landmark matching harmonic maps by looking for the best vector fields minimizing a shape energy. The use of vector fields to compute the registration makes the optimization easier, although it cannot describe all surface maps. An advantage of this method is that exact landmark matching can be guaranteed. Time dependent vector fields can also be used [22, 12, 13, 9, 10]. For example, Glaun  s et al. [12] proposed to generate large deformation diffeomorphisms of a sphere, with given displacements of a finite set of template landmarks. The time dependent vector fields facilitate the optimization procedure, although it may not be a good representation of surface maps since it requires more memory. The computational cost of the algorithm is also expensive. Quasi-conformal mapping that matches landmarks consistently has also been proposed. Wei et al. [42] also proposed to compute quasi-conformal mappings for feature matching face registration. The Beltrami coefficient associated to a landmark-matching parameterization is approximated. However, neither exact landmark matching nor the bijectivity of the mapping can be guaranteed, especially when very large deformations occur.

Algorithms for hybrid registration, which combines both the landmark and intensity information to guide the registration, has also been proposed[33][2][17][21][11].

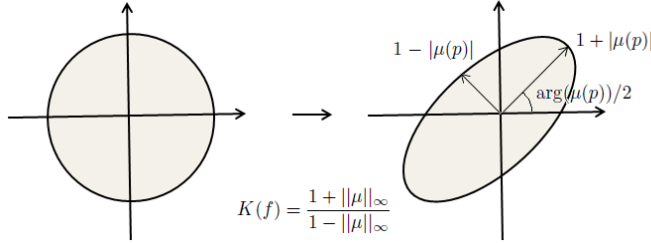


Fig. 3.1: Illustration of how the Beltrami coefficient determines the conformality distortion.

For example, Christensen et al. [21] proposed an algorithm for hybrid registration that uses both landmark and intensity information to guide the registration. The method utilizes the unidirectional landmark thin-plate spline (UL-TPS) registration technique together with a minimization scheme for the intensity difference to obtain good correspondence between images. Glocker et al. [11] proposed a hybrid image registration paradigm with a coupled formulation of two energy functionals that measure landmark and intensity mismatching. The algorithm exploits the Markov random field formulation to match image intensity and uses a discrete optimization technique to minimize the coupled energy. Paquin et al. [33] proposed a registration method using a hybrid combination of coarse-scale landmark and B-splines deformable registration techniques. Chanwimaluang et al. [2] proposed a hybrid retinal image registration approach that combines both area-based and feature-based methods. Existing hybrid registration techniques can drive data into good correspondence when deformations are not too large. In this work, we propose a hybrid quasi-conformal registration method, which can deal with very large deformations.

**3. Mathematical background.** In this work, we apply quasi-conformal maps to obtain diffeomorphic registrations with large deformations. In this section, we describe some basic theories related to quasi-conformal geometry. For details, we refer readers to [4][23].

A surface  $S$  with a conformal structure is called a *Riemann surface*. Given two Riemann surfaces  $M$  and  $N$ , a map  $f : M \rightarrow N$  is *conformal* if it preserves the surface metric up to a multiplicative factor called the *conformal factor*. An immediate consequence is that every conformal map preserves angles. With the angle-preserving property, a conformal map effectively preserves the local geometry of the surface structure. A generalization of conformal maps is the *quasi-conformal* maps, which are orientation preserving homeomorphisms between Riemann surfaces with bounded conformality distortion, in the sense that their first order approximations take small circles to small ellipses of bounded eccentricity [4]. Mathematically,  $f : \mathbb{C} \rightarrow \mathbb{C}$  is quasi-conformal provided that it satisfies the Beltrami equation:

$$\frac{\partial f}{\partial \bar{z}} = \mu(z) \frac{\partial f}{\partial z}. \quad (3.1)$$

for some complex-valued function  $\mu$  satisfying  $\|\mu\|_\infty < 1$ .  $\mu$  is called the *Beltrami coefficient*, which is a measure of non-conformality. It measures how far the map at each point is deviated from a conformal map. In particular, the map  $f$  is conformal around a small neighborhood of  $p$  when  $\mu(p) = 0$ . Infinitesimally, around a point  $p$ ,

$f$  may be expressed with respect to its local parameter as follows:

$$\begin{aligned} f(z) &= f(p) + f_z(p)z + f_{\bar{z}}(p)\bar{z} \\ &= f(p) + f_z(p)(z + \mu(p)\bar{z}). \end{aligned} \quad (3.2)$$

Obviously,  $f$  is not conformal if and only if  $\mu(p) \neq 0$ . Inside the local parameter domain,  $f$  may be considered as a map composed of a translation to  $f(p)$  together with a stretch map  $S(z) = z + \mu(p)\bar{z}$ , which is postcomposed by a multiplication of  $f_z(p)$ , which is conformal. All the conformal distortion of  $S(z)$  is caused by  $\mu(p)$ .  $S(z)$  is the map that causes  $f$  to map a small circle to a small ellipse. From  $\mu(p)$ , we can determine the angles of the directions of maximal magnification and shrinking and the amount of them as well. Specifically, the angle of maximal magnification is  $\arg(\mu(p))/2$  with magnifying factor  $1 + |\mu(p)|$ ; The angle of maximal shrinking is the orthogonal angle  $(\arg(\mu(p)) - \pi)/2$  with shrinking factor  $1 - |\mu(p)|$ . Thus, the Beltrami coefficient  $\mu$  gives us lots of information about the properties of the map (See Figure 3.1).

The maximal dilation of  $f$  is given by:

$$K(f) = \frac{1 + \|\mu\|_\infty}{1 - \|\mu\|_\infty}. \quad (3.3)$$

Given a Beltrami coefficient  $\mu : \mathbb{C} \rightarrow \mathbb{C}$  with  $\|\mu\|_\infty < 1$ . There is always a quasiconformal mapping from  $\mathbb{C}$  onto itself which satisfies the Beltrami equation in the distribution sense [4]. More precisely,

**Theorem 3.1** (Measurable Riemann Mapping Theorem). *Suppose  $\mu : \mathbb{C} \rightarrow \mathbb{C}$  is Lebesgue measurable satisfying  $\|\mu\|_\infty < 1$ , then there is a quasiconformal homeomorphism  $\phi$  from  $\mathbb{C}$  onto itself, which is in the Sobolev space  $W^{1,2}(\mathbb{C})$  and satisfied the Beltrami equation 3.1 in the distribution sense. Furthermore, by fixing 0, 1 and  $\infty$ , the associated quasiconformal homeomorphism  $\phi$  is uniquely determined.*

By reflection, the above theorem can be further extended to Beltrami coefficients defined on the unit disk  $\mathbb{D}$ .

**Theorem 3.2.** *Suppose  $\mu : \mathbb{D} \rightarrow \mathbb{C}$  is Lebesgue measurable satisfying  $\|\mu\|_\infty < 1$ , then there is a quasiconformal homeomorphism  $\phi$  from the unit disk to itself, which is in the Sobolev space  $W^{1,2}(\Omega)$  and satisfied the Beltrami equation 3.1 in the distribution sense. Furthermore, by fixing 0 and 1, the associated quasiconformal homeomorphism  $\phi$  is uniquely determined.*

Theorem 3.1 and Theorem 3.2 suggest that under suitable normalization, a homeomorphism from  $\mathbb{C}$  or  $\mathbb{D}$  onto itself can be uniquely determined by its associated Beltrami coefficient (See Figure 3.2).

Quasiconformal mapping between two Riemann surfaces  $S_1$  and  $S_2$  can also be defined. Instead of the Beltrami coefficient, the *Beltrami differential* is used. A Beltrami differential  $\mu(z) \frac{dz}{dz}$  on a Riemann surface  $S$  is an assignment to each chart  $(U_\alpha, \phi_\alpha)$  of an  $L_\infty$  complex-valued function  $\mu_\alpha$ , defined on local parameter  $z_\alpha$  such that

$$\mu_\alpha(z_\alpha) \frac{d\bar{z}_\alpha}{dz_\alpha} = \mu_\beta(z_\beta) \frac{d\bar{z}_\beta}{dz_\beta}, \quad (3.4)$$

on the domain which is also covered by another chart  $(U_\beta, \phi_\beta)$ . Here,  $\frac{dz_\beta}{dz_\alpha} = \frac{d}{dz_\alpha} \phi_{\alpha\beta}$  and  $\phi_{\alpha\beta} = \phi_\beta \circ \phi_\alpha^{-1}$ .

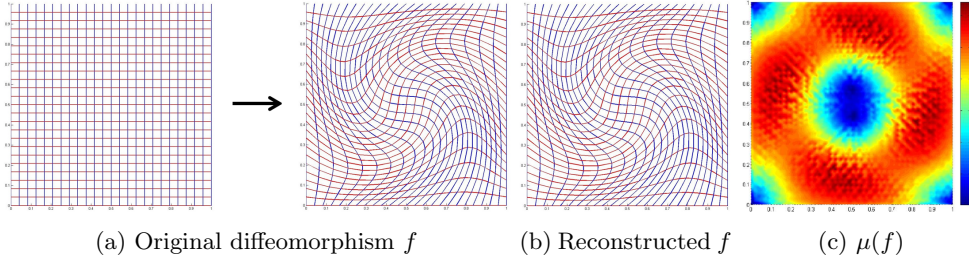


Fig. 3.2: Reconstruction of a diffeomorphism  $f$  from its associated Beltrami coefficient  $\mu$ . (a) shows a diffeomorphism between two rectangles. Its Beltrami coefficient is computed. (b) shows the reconstructed quasi-conformal map from the Beltrami coefficient. (c) shows the norm of the Beltrami coefficient.

An orientation preserving diffeomorphism  $f : S_1 \rightarrow S_2$  is called quasi-conformal associated with  $\mu(z) \frac{dz}{dz}$  if for any chart  $(U_\alpha, \phi_\alpha)$  on  $S_1$  and any chart  $(V_\beta, \psi_\beta)$  on  $S_2$ , the mapping  $f_{\alpha\beta} := \psi_\beta \circ f \circ \phi_\alpha^{-1}$  is quasi-conformal associated with  $\mu_\alpha(z_\alpha) \frac{dz_\alpha}{dz_\alpha}$ .

**4. Proposed algorithm.** In this section, we explain our proposed model for diffeomorphic registration with large deformations in details. The basic idea is to look for a quasi-conformal map to register two corresponding data, which can either be images or surfaces. The quasi-conformal map is obtained by minimizing an energy functional involving a Beltrami coefficient term, which measures the distortion of the quasi-conformal map. The Beltrami coefficient effectively controls the bijectivity and smoothness of the registration, even with very large deformations.

**4.1. Proposed model.** Let  $S_1$  and  $S_2$  be two corresponding images or surfaces. Our goal is to find a smooth and bijective mapping  $f : S_1 \rightarrow S_2$  between  $S_1$  and  $S_2$  satisfying certain prescribed criteria. For landmark-based registration, we look for a registration that matches corresponding feature landmarks. Let  $\{p_i \in S_1\}_{i=1}^m$  and  $\{q_i \in S_2\}_{i=1}^m$  be the sets of corresponding feature landmarks defined on  $S_1$  and  $S_2$  respectively. We search for a diffeomorphism  $f : S_1 \rightarrow S_2$  subject to the landmark constraints that  $f(p_i) = q_i$  for all  $1 \leq i \leq m$ .

We propose a variational approach to obtain an optimized quasi-conformal map  $f$ , which minimizes an energy functional  $E_{LM}$  involving the Beltrami coefficient terms. More specifically, we propose to solve the following minimization problem:

$$\begin{aligned} f &= \arg \min_{g: S_1 \rightarrow S_2} E_{LM}(\mu_g) \\ &:= \arg \min_{g: S_1 \rightarrow S_2} \left\{ \int_{S_1} |\nabla \mu_g|^2 + \alpha \int_{S_1} |\mu_g|^p \right\} \end{aligned} \quad (4.1)$$

subject to the constraints that:

- C(i)  $f(p_i) = q_i$  for  $1 \leq i \leq m$  (landmark constraint);
- C(ii)  $\|\mu_f\|_\infty < 1$  (bijectivity),

where  $\mu_f$  and  $\mu_g$  are the Beltrami coefficients of  $f$  and  $g$  respectively.

The first term of  $E_{LM}$  ensures the smoothness of  $f$ . The second term of  $E_{LM}$  aims to minimize the conformality distortion of  $f$ . The constraint C(i) is the landmark constraint, which enforces  $f$  to match corresponding landmarks consistently.

**PROPOSITION 4.1.** *If  $f : S_1 \rightarrow S_2$  is a  $C^1$  map satisfying the constraint C(ii), then  $f$  is bijective.*

*Proof.* Suppose  $f = u + iv$  under some local coordinates. The Beltrami coefficient  $\mu_f$  is given by:

$$\mu_f = \frac{\partial f}{\partial \bar{z}} / \frac{\partial f}{\partial z} \quad (4.2)$$

where

$$\frac{\partial f}{\partial \bar{z}} = \frac{(u_x - v_y) + i(u_y + v_x)}{2}; \quad \frac{\partial f}{\partial z} = \frac{(u_x + v_y) + i(v_x + u_y)}{2}; \quad (4.3)$$

Now, the Jacobian of  $f$ ,  $J_f$ , is given by:

$$\begin{aligned} J_f &= u_x v_y - u_y v_x \\ &= \frac{(u_x + v_y)^2 + (v_x + u_y)^2 - (u_x - v_y)^2 - (u_y + v_x)^2}{4} \\ &= \left| \frac{\partial f}{\partial z} \right|^2 - \left| \frac{\partial f}{\partial \bar{z}} \right|^2 = \left| \frac{\partial f}{\partial z} \right|^2 (1 - |\mu_f|^2) \end{aligned} \quad (4.4)$$

Since  $\|\mu_f\|_\infty < 1$ ,  $\left| \frac{\partial f}{\partial z} \right|^2 \neq 0$ . Also,  $(1 - |\mu_f|^2) > 0$ . Hence,  $J_f > 0$  everywhere.

Since the Jacobian is positive everywhere, by the inverse function theorem, the mapping  $f$  is locally invertible everywhere. In other words,  $f$  is bijective.  $\square$

In other words, C(ii) is the condition to ensure the obtained registration is bijective. In practice, this condition is automatically satisfied by minimizing the second term of  $E_{LM}$  for large enough  $p$ . In all of our experiments, we choose  $p = 2$  and the method is able to obtain a bijective registration satisfying the condition C(ii).

In order to improve the accuracy of the registration, one can combine the landmark-matching registration model with the intensity matching model. The intensities are functions defined on  $S_1$  and  $S_2$ . Usually, they are image intensities for image registration and surface curvatures for surface registration. Ideally, we want to obtain a landmark-matching diffeomorphism  $f : S_1 \rightarrow S_2$  that matches the intensities as much as possible. We denote the intensities on  $S_1$  and  $S_2$  by  $I_1 : S_1 \rightarrow \mathbb{R}$  and  $I_2 : S_2 \rightarrow \mathbb{R}$  respectively. Our registration model can be modified as solving the following minimization problem:

$$\begin{aligned} f &= \arg \min_{g: S_1 \rightarrow S_2} E_{IM}(g) \\ &:= \arg \min_{g: S_1 \rightarrow S_2} \left\{ \int_{S_1} |\nabla \mu_g|^2 + \alpha \int_{S_1} |\mu_g|^p + \beta \int_{S_1} (I_1 - I_2(g))^2 \right\} \end{aligned} \quad (4.5)$$

subject to the constraints C(i) and C(ii).

**4.2. Energy minimization.** In this subsection, we describe an algorithm to approximate the solutions of the above minimization problems.

**4.2.1. Landmark-based registration model.** Given two corresponding sets of landmarks  $\{p_i\}_{i=1}^n$  and  $\{q_i\}_{i=1}^n$  on  $S_1$  and  $S_2$  respectively, our goal is to look for a diffeomorphism  $f : S_1 \rightarrow S_2$  that satisfies  $f(p_i) = q_i$  ( $i = 1, \dots, n$ ) while minimizing the local geometric distortion. Our proposed model is to solve the variational problem (4.1) as described in the last subsection.

More specifically, our goal is to look for an optimal Beltrami coefficient  $\nu : S_1 \rightarrow \mathbb{C}$ , which is the Beltrami coefficient of some diffeomorphism  $f : S_1 \rightarrow S_2$ , minimizing the following energy functional  $E_{LM}$ :

$$E_{LM}(\nu) = \int_{S_1} |\nabla \nu|^2 + \alpha \int_{S_1} |\nu|^p \quad (4.6)$$

subject to the constraints that  $\|\nu\|_\infty < 1$ ,  $f(p_i) = q_i$  for  $i = 1, 2, \dots, n$  and  $\nu = \mu(f)$ , where  $\mu(f)$  is the Beltrami coefficient of  $f$ .

We apply a splitting method to solve the constrained optimization problem. In particular, we consider to minimize:

$$E_{LM}^{split}(\nu, f) = \int_{S_1} |\nabla \nu|^2 + \alpha \int_{S_1} |\nu|^p + \sigma \int_{S_1} |\nu - \mu(f)|^2 \quad (4.7)$$

subject to the constraints that  $\|\nu\|_\infty < 1$  and  $f(p_i) = q_i$  for  $i = 1, 2, \dots, n$ .

We iteratively minimize  $E_{LM}^{split}$  subject to the constraints. Set  $\nu_0 = 0$ . Suppose  $\nu_n$  is obtained at the  $n^{th}$  iteration. Fixing  $\nu_n$ , we minimize  $E_{LM}^{split}(\nu_n, f)$  over  $f$ , subject to the constraint that  $f(p_i) = q_i$  ( $i = 1, 2, \dots, n$ ), to obtain  $f_n$ . Once  $f_n$  is obtained, by fixing  $f_n$ , we minimize  $E_{LM}^{split}(\nu, f_n)$  over  $\nu$  to obtain  $\nu_{n+1}$ .

To minimize  $E_{LM}^{split}(\nu_n, f)$  over  $f$  fixing  $\nu_n$ , it is equivalent to finding a landmark matching diffeomorphism  $f_n : S_1 \rightarrow S_2$ , whose Beltrami coefficient closely resembles to  $\nu_n$  and satisfies the landmark constraints  $f(p_i) = q_i$ . To obtain such  $f_n$ , we propose to use the *Linear Beltrami Solver (LBS)* to find  $f_n$  such that  $f_n$  matches landmark constraints and its Beltrami coefficient closely resembles to  $\nu_n$ .

Let  $f = u + iv$ . From the Beltrami equation (3.1),

$$\mu(f) = \frac{(u_x - v_y) + i(v_x + u_y)}{(u_x + v_y) + i(v_x - u_y)} \quad (4.8)$$

Let  $\mu(f) = \rho + i\tau$ . We can write  $v_x$  and  $v_y$  as linear combinations of  $u_x$  and  $u_y$ ,

$$\begin{aligned} -v_y &= \alpha_1 u_x + \alpha_2 u_y; \\ v_x &= \alpha_2 u_x + \alpha_3 u_y. \end{aligned} \quad (4.9)$$

where  $\alpha_1 = \frac{(\rho-1)^2 + \tau^2}{1-\rho^2-\tau^2}$ ;  $\alpha_2 = -\frac{2\tau}{1-\rho^2-\tau^2}$ ;  $\alpha_3 = \frac{1+2\rho+\rho^2+\tau^2}{1-\rho^2-\tau^2}$ .

Similarly,

$$\begin{aligned} u_y &= \alpha_1 v_x + \alpha_2 v_y; \\ -u_x &= \alpha_2 v_x + \alpha_3 v_y. \end{aligned} \quad (4.10)$$

Since  $\nabla \cdot \begin{pmatrix} -v_y \\ v_x \end{pmatrix} = 0$  and  $\nabla \cdot \begin{pmatrix} u_y \\ -u_x \end{pmatrix} = 0$ , we obtain

$$\nabla \cdot \left( A \begin{pmatrix} u_x \\ u_y \end{pmatrix} \right) = 0 \quad \text{and} \quad \nabla \cdot \left( A \begin{pmatrix} v_x \\ v_y \end{pmatrix} \right) = 0 \quad (4.11)$$

where  $A = \begin{pmatrix} \alpha_1 & \alpha_2 \\ \alpha_2 & \alpha_3 \end{pmatrix}$ .

In the discrete case, the elliptic PDEs (4.11) can be discretized into sparse positive definite linear systems. Given  $\nu_n$  and the landmark constraints, one can solve the

linear systems with the landmark constraints in the least square sense. A landmark matching quasi-conformal map  $f_n$ , whose Beltrami coefficient closely resembles to  $\nu_n$ , can then be obtained.

Once  $f_n$  is obtained, we minimize  $E_{LM}^{split}(\nu, f_n)$  over  $\nu$  while fixing  $f_n$ . In other words, we look for  $\nu_{n+1}$  minimizing:

$$\int_{S_1} |\nabla \nu|^2 + \alpha \int_{S_1} |\nu|^p + \sigma \int_{S_1} |\nu - \mu(f_n)|^2 \quad (4.12)$$

In the case when  $p = 2$ , by considering the Euler-Lagrange equation, it is equivalent to solving:

$$(\Delta + 2\alpha I + 2\sigma I)\nu_{n+1} = \mu(f_n) \quad (4.13)$$

In discrete case, equation (4.13) can be discretized into a sparse linear system and can be solved efficiently. However, the Beltrami coefficient  $\nu_{n+1}$  obtained by solving (4.13) might not be associated to a landmark-matching quasi-conformal map. To minimize the landmark mismatching error, we use the LBS with  $\nu_{n+1}$  as the input together with the landmark constraints to obtain a landmark-matching quasi-conformal map  $\tilde{f}_{n+1}$ , whose Beltrami coefficient  $\nu_{n+1}$  closely resembles to  $\nu_{n+1}$ . Using  $d = \nu_{n+1} - \nu_{n+1}$  as a descent direction, we update  $\nu_n$  from the solution of the Equation (4.13) by  $\nu_{n+1} \leftarrow \nu_{n+1} + td$  for some small  $t$ . This gives a smooth  $\nu_{n+1}$  and the landmark-mismatching error can be reduced.

We keep the iteration going to obtain a sequence of pair  $\{(\nu_i, f_i)\}_{i=1}^\infty$ . The iteration stops when  $\|\nu_{n+1} - \nu_n\|_\infty \leq \epsilon$  for some small threshold  $\epsilon$ . Theoretically, the conventional penalty method requires that  $\sigma$  increases to infinity. In practice, we increases  $\sigma$  in each iteration and the algorithm can give satisfactory results.

In summary, the proposed landmark-based registration model can be described as follows:

---

**Algorithm 1:** Landmark-based registration

---

**Input:** Images or surfaces:  $S_1$  and  $S_2$ ; landmark sets  $\{p_i \in S_1\}_{i=1}^m$  and  $\{q_i \in S_2\}_{i=1}^m$ .

**Output:** Optimal Beltrami coefficient  $\nu^*$ ; Landmark-matching  $f^* : S_1 \rightarrow S_2$ .

- 1 Initial  $\nu_0 = 0$ ;
  - 2 **repeat**
  - 3    Use LBS to reconstruct  $f_n$  from  $\nu_n$  with landmark constraints;
  - 4    Fix  $f_n$ , obtain  $\nu_{n+1}$  by solving:
  - 5     
$$\nu_{n+1} = \arg \min_{\nu} \left\{ \int |\nabla \nu|^2 + \alpha \int |\nu|^p + \sigma \int |\nu - \mu(f_n)|^2 \right\};$$
  - 6    Use LBS to obtain  $\tilde{f}_{n+1}$  from  $\nu_{n+1}$  with landmark constraints;
  - 7    Compute  $d = \mu(\tilde{f}_{n+1}) - \nu_{n+1}$ ;
  - 8     $\nu_{n+1} \leftarrow \nu_{n+1} + td$  for some small  $t$ ;
  - 9 **until**  $\|\nu_{n+1} - \nu_n\|_\infty \leq \epsilon$ ;
-

**4.2.2. Hybrid registration model.** The proposed landmark-based registration model can also be combined with matching intensity (such as image intensity for image registration or surface curvature for surface registration) to improve the accuracy of the registration result. More specifically, our goal is to look for an optimal Beltrami coefficient  $\nu : S_1 \rightarrow \mathbb{C}$ , which is associated to a diffeomorphism  $f : S_1 \rightarrow S_2$ , minimizing the following energy functional  $E_{IM}$ :

$$E_{IM}(\nu, f) = \int_{S_1} |\nabla \nu|^2 + \alpha \int_{S_1} |\nu|^p + \beta \int_{S_1} (I_1 - I_2(f))^2 \quad (4.14)$$

subject to the constraints that  $\|\nu\|_\infty < 1$  and  $f(p_i) = q_i$  for  $i = 1, 2, \dots, n$ . Here,  $I_1$  and  $I_2$  are the intensity functions defined on  $S_1$  and  $S_2$  respectively.

We again apply a splitting method to solve the above constrained optimization problem. We consider to minimize:

$$\begin{aligned} E_{IM}^{split}(\nu, \mu) = & \int_{S_1} |\nabla \nu|^2 + \alpha \int_{S_1} |\nu|^p + \sigma \int_{S_1} |\nu - \mu|^2 \\ & + \beta \int_{S_1} (I_1 - I_2(f^\mu))^2 \end{aligned} \quad (4.15)$$

subject to the constraints that  $\|\nu\|_\infty < 1$  and  $f^\mu$  is the quasi-conformal map with Beltrami coefficient  $\mu$  satisfying  $f^\mu(p_i) = q_i$  for  $i = 1, 2, \dots, n$ .

To solve the above optimization problem, we iteratively minimize  $E_{IM}^{split}$  subject to the constraints. Set  $\nu_0 = 0$  and use the LBS to reconstruct  $f_0$  from  $\tilde{\mu}_0 := 0$  satisfying the landmark constraints. Set  $\mu_0 = \mu(f_0)$ . Suppose  $\nu_n$  and  $\mu_n$  is obtained at the  $n^{th}$  iteration. Fixing  $\nu_n$ , we minimize  $E_{IM}^{split}(\nu_n, \mu)$  over  $\mu$ , subject to the constraint that  $f^\mu(p_i) = q_i$  ( $i = 1, 2, \dots, n$ ), to obtain  $\mu_{n+1}$ . Once  $\mu_{n+1}$  is obtained, fixing  $\mu_{n+1}$ , we minimize  $E_{IM}^{split}(\nu, \mu_{n+1})$  over  $\nu$  to obtain  $\nu_{n+1}$ .

We first discuss the minimization  $E_{IM}^{split}(\nu_n, \mu)$  over  $\mu$  fixing  $\nu_n$ , subject to the constraint that  $f^\mu(p_i) = q_i$  ( $i = 1, 2, \dots, n$ ). This problem is equivalent to solving:

$$\mu_{n+1} = \arg \min_{\mu} \left\{ \beta \int_{S_1} (I_1 - I_2(f^\mu))^2 + \sigma \int_{S_1} |\mu - \nu_n|^2 \right\} \quad (4.16)$$

Using the gradient descent method, we compute the descent direction  $df$ , which minimizes  $\int_{S_1} (I_1 - I_2(f^\mu))^2$ . The descent direction  $df$  is given by:

$$df = 2(I_1 - I_2(f^\mu))\nabla I_2(f^\mu). \quad (4.17)$$

As  $f^\mu$  is perturbed, its associated Beltrami coefficient is also adjusted by  $d\mu_1$ . The adjustment can be explicitly computed. Note that:

$$\frac{\partial(f + df)}{\partial \bar{z}} = (\mu + d\mu_1) \frac{\partial(f + df)}{\partial z} \quad (4.18)$$

which implies:

$$\frac{\partial f}{\partial \bar{z}} + \frac{\partial df}{\partial \bar{z}} = \mu \frac{\partial f}{\partial z} + d\mu_1 \frac{\partial f}{\partial z} + \mu \frac{\partial df}{\partial z} + d\mu_1 \frac{\partial df}{\partial z} \quad (4.19)$$

Note that  $\frac{\partial f}{\partial \bar{z}} = \mu \frac{\partial f}{\partial z}$ . Thus, the adjustment  $d\mu_1$  can be obtained by:

$$d\mu_1 = \left( \frac{\partial df}{\partial \bar{z}} - \mu \frac{\partial df}{\partial z} \right) / \frac{\partial(f + df)}{\partial z} \quad (4.20)$$

Similarly, we can obtain the descent direction  $d\mu_2$  that minimizes  $\int_{S_1} |\mu - \nu_n|^2$ .  $d\mu_2$  is given by:

$$d\mu_2 = -2(\mu - \nu_n). \quad (4.21)$$

Therefore, the descent direction to solve the optimization problem (4.16) is given by:

$$d\mu = \beta d\mu_1 + \sigma d\mu_2 \quad (4.22)$$

Using the above formula for the descent direction, we obtain an updated Beltrami coefficient:

$$\tilde{\mu}_{n+1} = \mu_n + d\mu \quad (4.23)$$

We then compute a quasi-conformal map  $f_{n+1}$ , whose Beltrami coefficient closely resembles to  $\tilde{\mu}_{n+1}$ , using LBS with the landmark constraints enforced. This step ensures a landmark matching registration can be obtained. We then update  $\mu_n$  by:  $\mu_{n+1} = \mu(f_{n+1})$ .

Once  $\mu_{n+1}$  is obtained, fixing  $\mu_{n+1}$ , we minimize  $E_{IM}^{split}(\nu, \mu_{n+1})$  over  $\nu$  to obtain  $\nu_{n+1}$ . In other words, we look for  $\nu_{n+1}$  minimizing:

$$\int_{S_1} |\nabla \nu|^2 + \alpha \int_{S_1} |\nu|^p + \sigma \int_{S_1} |\nu - \mu_{n+1}|^2 \quad (4.24)$$

In the case when  $p = 2$ , by considering the Euler-Lagrange equation, it is equivalent to solving:

$$(\Delta + 2\alpha I + 2\sigma I)\nu_{n+1} = \mu_{n+1} \quad (4.25)$$

In discrete case, equation (4.25) can be discretized into a sparse linear system and can be solved efficiently. Similar to section 4.2.1, we use the LBS with  $\nu_{n+1}$  as the input together with the landmark constraints to obtain a descent direction  $d$  to update  $\nu_{n+1}$  by  $\nu_{n+1} \leftarrow \nu_{n+1} + td$  for some small  $t$ . This gives a smooth  $\nu_n$  and the landmark-mismatching error will be reduced.

We keep the iteration going to obtain a sequence of pair  $\{(\nu_n, \mu_n)\}_{n=1}^\infty$ . The iteration stops when  $\|\mu_{n+1} - \mu_n\|_\infty \leq \epsilon$  for some small threshold  $\epsilon$ . Again, the conventional penalty method requires that  $\sigma$  increases to infinity. However, in practice, we increase  $\sigma$  in each iteration and the algorithm can give satisfactory results.

We call this proposed algorithm *Q-Fibra*, which refers to quasi-conformal feature and intensity-based registration algorithm. In summary, the proposed Q-Fibra hybrid registration model can be described as follows:

**5. Numerical implementation.** The proposed models for landmark-based and hybrid registration rely on the Linear Beltrami Solver(LBS) and solving the Euler-Lagrange(E-L) equations. In this section, we will describe the numerical implementation of the LBS and also the discretizations of the E-L equations.

Practically speaking, 2D domains or surfaces in  $\mathbb{R}^3$  are usually represented discretely by triangular meshes. Suppose  $K_1$  and  $K_2$  are two surface meshes with the same topology representing  $S_1$  and  $S_2$ . We define the set of vertices on  $K_1$  and  $K_2$  by  $V^1 = \{v_i^1\}_{i=1}^n$  and  $V^2 = \{v_i^2\}_{i=1}^n$  respectively. Similarly, we define the set of triangular faces on  $K_1$  and  $K_2$  by  $F^1 = \{T_j^1\}_{j=1}^m$  and  $F^2 = \{T_j^2\}_{j=1}^m$ .

**Algorithm 2:** Q-Fibra Hybrid registration

---

**Input:** Images or surfaces:  $S_1$  and  $S_2$ ; landmark sets  $\{p_i \in S_1\}_{i=1}^m$  and  $\{q_i \in S_2\}_{i=1}^m$ ; intensity functions  $I_1$  and  $I_2$  defined on  $S_1$  and  $S_2$  respectively.

**Output:** Optimal Beltrami coefficient  $\nu^*$ ; hybrid registration  $f^* : S_1 \rightarrow S_2$ .

- 1 Initial  $\nu_0 = 0$ ,  $\tilde{\mu}_0 = 0$ ;
  - 2 Use LBS to reconstruct  $f_0$  from  $\tilde{\mu}_0 = 0$  with landmark constraints;
  - 3 Initial  $\mu_0 = \mu(f_0)$ ;
  - 4 **repeat**
  - 5     Given  $\nu_n, \mu_n$ . Fix  $\nu_n$  and obtain  $\tilde{\mu}_{n+1}$  by solving:  

$$\tilde{\mu}_{n+1} = \arg \min_{\mu} \left\{ \beta \int_{S_1} (I_1 - I_2(f^\mu))^2 + \sigma \int_{S_1} |\mu - \nu_n|^2 \right\};$$
  - 6     Use LBS to reconstruct  $f_{n+1}$  from  $\tilde{\mu}_{n+1}$  with landmark constraints;
  - 7      $\mu_{n+1} \leftarrow \mu(f_{n+1})$ ;
  - 8     Fix  $\mu_{n+1}$  and obtain  $\nu_{n+1}$  by solving:  

$$\nu_{n+1} = \arg \min_{\nu} \left\{ \int |\nabla \nu|^2 + \alpha \int |\nu|^p + \sigma \int |\nu - \mu(f_n)|^2 \right\};$$
  - 9     Use LBS to reconstruct  $\tilde{f}_{n+1}$  from  $\nu_{n+1}$  with landmark constraints;
  - 10    Compute  $d = \mu(\tilde{f}_{n+1}) - \nu_{n+1}$ ;
  - 11     $\nu_{n+1} \leftarrow \nu_{n+1} + td$  for some small  $t$ ;
  - 12 **until**  $\|\nu_{n+1} - \nu_n\|_\infty \leq \epsilon$ ;
- 

**5.1. Numerical details of LBS.** Suppose  $f : K_1 \rightarrow K_2$  is an orientation preserving piecewise linear homeomorphism between  $K_1$  and  $K_2$ . We can assume  $K_1$  and  $K_2$  are both embedded in  $\mathbb{R}^2$ . In case  $K_1$  and  $K_2$  are surface meshes in  $\mathbb{R}^3$ , we first parameterize them conformally by  $\phi_1 : K_1 \rightarrow D_1 \subseteq \mathbb{R}^2$  and  $\phi_2 : K_2 \rightarrow D_2 \subseteq \mathbb{R}^2$ . The composition of  $f$  with the conformal parameterizations,  $\tilde{f} := \phi_2 \circ f \circ \phi_1^{-1}$ , is then an orientation preserving piecewise linear homeomorphism between  $D_1$  and  $D_2$  embedded in  $\mathbb{R}^2$ .

To compute the quasi-conformal mapping, the key idea is to discretize Equation (4.11) with two linear systems.

Given a map  $f = (u + iv) : K_1 \rightarrow K_2$ , we can easily compute its associated Beltrami coefficient  $\mu_f$ , which is a complex-valued function defined on each triangular faces of  $K_1$ . To compute  $\mu_f$ , we simply need to approximate the partial derivatives on every face  $T$ . We denote them by  $D_x f(T) = D_x u + iD_x v$  and  $D_y f(T) = D_y u + iD_y v$  respectively. Note that  $f$  is piecewise linear. The restriction of  $f$  on each triangular face  $T$  can be written as:

$$f|_T(x, y) = \begin{pmatrix} a_T x + b_T y + r_T \\ c_T x + d_T y + s_T \end{pmatrix} \quad (5.1)$$

Hence,  $D_x u(T) = a_T$ ,  $D_y u(T) = b_T$ ,  $D_x v(T) = c_T$  and  $D_y v(T) = d_T$ . Now, the

gradient:

$$\nabla_T f := \begin{pmatrix} D_x f(T) \\ D_y f(T) \end{pmatrix} \quad (5.2)$$

on each face  $T$  can be computed by solving the linear system:

$$\begin{pmatrix} \vec{v}_1 - \vec{v}_0 \\ \vec{v}_2 - \vec{v}_0 \end{pmatrix} \nabla_T \tilde{f}_i = \begin{pmatrix} \frac{\tilde{f}_i(\vec{v}_1) - \tilde{f}_i(\vec{v}_0)}{|\vec{v}_1 - \vec{v}_0|} \\ \frac{\tilde{f}_i(\vec{v}_2) - \tilde{f}_i(\vec{v}_0)}{|\vec{v}_2 - \vec{v}_0|} \end{pmatrix}, \quad (5.3)$$

where  $[\vec{v}_0, \vec{v}_1]$  and  $[\vec{v}_0, \vec{v}_2]$  are two edges on  $T$ . By solving equation (5.3),  $a_T, b_T, c_T$  and  $d_T$  can be obtained. The Beltrami coefficient  $\mu_f(T)$  of the triangular face  $T$  can then be computed from the Beltrami equation (3.1) by:

$$\mu_f(T) = \frac{(a_T - d_T) + i(c_T + b_T)}{(a_T + d_T) + i(c_T - b_T)}, \quad (5.4)$$

Equation (4.9) and (4.10) are both satisfied on every triangular faces. Let  $\mu_f(T) = \rho_T + i \tau_T$ . The discrete versions of Equation (4.9) and (4.10) can be obtained.

$$\begin{aligned} -d_T &= \alpha_1(T)a_T + \alpha_2(T)b_T \\ c_T &= \alpha_2(T)a_T + \alpha_3(T)b_T \end{aligned} \quad (5.5)$$

and

$$\begin{aligned} -b_T &= \alpha_1(T)c_T + \alpha_2(T)d_T \\ a_T &= \alpha_2(T)c_T + \alpha_3(T)d_T \end{aligned} \quad (5.6)$$

where:  $\alpha_1(T) = \frac{(\rho_T - 1)^2 + \tau_T^2}{1 - \rho_T^2 - \tau_T^2}$ ;  $\alpha_2(T) = -\frac{2\tau_T}{1 - \rho_T^2 - \tau_T^2}$  and  
 $\alpha_3(T) = \frac{1 + 2\rho_T + \rho_T^2 + \tau_T^2}{1 - \rho_T^2 - \tau_T^2}$ .

In order to discretize Equation (4.11), we need to introduce the *discrete divergence*. The discrete divergence can be defined as follows. Let  $T = [v_i, v_j, v_k]$  and  $w_I = f(v_I)$  where  $I = i, j$  or  $k$ . Suppose  $v_I = g_I + i h_I$  and  $w_I = s_I + i t_I$  ( $I = i, j, k$ ). Using equation (5.3),  $a_T, b_T, c_T$  and  $d_T$  can be written as follows:

$$\begin{aligned} a_T &= A_i^T s_i + A_j^T s_j + A_k^T s_k; \\ b_T &= B_i^T s_i + B_j^T s_j + B_k^T s_k; \\ c_T &= A_i^T t_i + A_j^T t_j + A_k^T t_k; \\ d_T &= B_i^T t_i + B_j^T t_j + B_k^T t_k; \end{aligned} \quad (5.7)$$

where:

$$\begin{aligned} A_i^T &= (h_j - h_k)/Area(T), \\ A_j^T &= (h_k - h_i)/Area(T), \\ A_k^T &= (h_i - h_j)/Area(T); \\ B_i^T &= (g_k - g_j)/Area(T), \\ B_j^T &= (g_i - g_k)/Area(T), \\ B_k^T &= (g_j - g_i)/Area(T); \end{aligned} \quad (5.8)$$

Suppose  $\vec{V} = (V_1, V_2)$  is a discrete vector field defined on every triangular faces. For each vertex  $v_i$ , let  $N_i$  be the collection of neighborhood faces attached to  $v_i$ . We define the discrete divergence  $\text{Div}$  of  $\vec{V}$  as follows:

$$\text{Div}(\vec{V})(v_i) = \sum_{T \in N_i} A_i^T V_1(T) + B_i^T V_2(T) \quad (5.9)$$

By careful checking, one can prove that

$$\sum_{T \in N_i} A_i^T b_T = \sum_{T \in N_i} B_i^T a_T; \quad \sum_{T \in N_i} A_i^T d_T = \sum_{T \in N_i} B_i^T c_T. \quad (5.10)$$

This gives,

$$\text{Div} \begin{pmatrix} -D_y u \\ D_x u \end{pmatrix} = 0 \quad \text{and} \quad \text{Div} \begin{pmatrix} -D_y v \\ D_x v \end{pmatrix} = 0 \quad (5.11)$$

As a result, Equation (4.11) can be discretized:

$$\text{Div} \left( A \begin{pmatrix} D_x u \\ D_y u \end{pmatrix} \right) = 0 \quad \text{and} \quad \text{Div} \left( A \begin{pmatrix} D_x v \\ D_y v \end{pmatrix} \right) = 0 \quad (5.12)$$

where  $A = \begin{pmatrix} \alpha_1 & \alpha_2 \\ \alpha_2 & \alpha_3 \end{pmatrix}$ . This is equivalent to:

$$\begin{aligned} \sum_{T \in N_i} A_i^T [\alpha_1(T)a_T + \alpha_2(T)b_T] + B_i^T [\alpha_2(T)a_T + \alpha_3(T)b_T] &= 0 \\ \sum_{T \in N_i} A_i^T [\alpha_1(T)c_T + \alpha_2(T)d_T] + B_i^T [\alpha_2(T)c_T + \alpha_3(T)d_T] &= 0 \end{aligned} \quad (5.13)$$

for all vertices  $v_i \in D$ . Note that  $a_T, b_T, c_T$  and  $d_T$  can be written as a linear combination of the x-coordinates and y-coordinate of the desired quasi-conformal map  $f$ . Hence, equation (5.13) gives us the linear systems to solve for the x-coordinate and y-coordinate function of  $f$ .

Besides,  $f$  has to satisfy certain constraints on the boundary. One common situation is to give the Dirichlet condition on the whole boundary. That is, for any  $v_b \in \partial K_1$

$$f(v_b) = w_b \in \partial K_2 \quad (5.14)$$

Note that the Dirichlet condition is not required to be enforced on the whole boundary. The proposed algorithm also allows free boundary condition. For example, in the case that  $K_1$  and  $K_2$  are rectangles, the desired quasi-conformal map should satisfy

$$\begin{aligned} f(0) &= 0; f(1) = 1; f(i) = i; f(1+i) = 1+i; \\ \mathbf{Re}(f) &= 0 \text{ on arc } [0, i]; \quad \mathbf{Re}(f) = 1 \text{ on arc } [1, 1+i]; \\ \mathbf{Imag}(f) &= 0 \text{ on arc } [0, 1]; \quad \mathbf{Imag}(f) = 1 \text{ on arc } [i, 1+i] \end{aligned} \quad (5.15)$$

Besides, in our case, interior landmark correspondences  $\{p_i\}_{i=1}^n \leftrightarrow \{q_i\}_{i=1}^n$  are also enforced. Thus, we should add this constraint to the linear systems. Mathematically, it is described as  $f(p_i) = q_i$  ( $i = 1, 2, \dots, n$ ).

**5.2. Discretization of E-L equation (4.13).** In both the landmark-based and Q-Fibra hybrid registration algorithms, solving Equation (4.13) to adjust the Beltrami coefficient is required. In this subsection, we describe how Equation (4.13) can be discretized.

In discrete case, the Beltrami coefficient  $\mu(T)$  is defined on each triangular face  $T$ . We first approximate the Beltrami coefficient  $\mu(v_i)$  at a vertex  $v_i$  by

$$\mu(v_i) = \frac{1}{N_i} \sum_{T \in N_i} \mu(T) \quad (5.16)$$

where  $N_i$  is the collection of neighborhood faces attached to  $v_i$ . In other words,  $\mu(v_i)$  is the average of the Beltrami coefficients  $\mu(T)$  on 1-ring neighbourhood triangles.

The discretization of Equation (4.13) can be done after discretizing the Laplacian operator  $\Delta$ . Let  $T_1 = [v_i, v_j, v_k]$  and  $T_2 = [v_i, v_j, v_l]$ . The mesh laplacian is defined as:

$$\Delta(f(v_i)) = \sum_{T \in N_i} \frac{\cot \alpha_{ij} + \cot \beta_{ij}}{2} (f(v_j) - f(v_i)) \quad (5.17)$$

where  $\alpha_{ij}$  and  $\beta_{ij}$  are the two interior angles of  $T_1$  and  $T_2$  which are opposite to the edge  $[v_i, v_j]$ . To find  $\alpha_{ij}$  and  $\beta_{ij}$ , we follow the idea of [19]. Let  $l_{ij}$  be the length of the edge  $[v_i, v_j]$ . By law of cosines:  $l_{ij}^2 = l_{jk}^2 + l_{ki}^2 - 2l_{jk}l_{ki} \cos \alpha_{ij}$ , we have

$$\cos \alpha_{ij} = \frac{-l_{ij}^2 + l_{jk}^2 + l_{ki}^2}{2l_{jk}l_{ki}}. \quad (5.18)$$

Similar, by the law of sines:  $\text{Area}(T_1) = \frac{1}{2}l_{jk}l_{ki} \sin \alpha_{ij}$ , we have

$$\sin \alpha_{ij} = \frac{2\text{Area}(T_1)}{l_{jk}l_{ki}}. \quad (5.19)$$

Therefore we have

$$\cot \alpha_{ij} = \frac{-l_{ij}^2 + l_{jk}^2 + l_{ki}^2}{4\text{Area}(T_1)} \quad (5.20)$$

and the discrete Laplacian operator can then be constructed. Similarly,  $\cot \beta_{ij}$  can be computed.

The solution  $\nu_{n+1}$  of the discretized Equation (4.13) is defined on each vertices. We have to approximate  $\nu_{n+1}(T)$  on each face  $T$  before proceeding to the next step . The approximation is taken to be

$$\nu_{n+1}(T) = \frac{1}{3} \sum_{v_i \in T} \nu_{n+1}(v_i) \quad (5.21)$$

**5.3. Numerical implementation for intensity-matching.** In Section 4.2.2, we propose the Q-Fibra hybrid registration algorithm, which requires to solve

$$\arg \min_{\mu} \left\{ \gamma \int_{S_1} (I_1 - I_2(f^\mu))^2 + \sigma \int_{S_1} |\mu - \nu_n|^2 \right\},$$

which can be solved using the gradient descent method. It involves calculating the gradient of  $\mu$ , which is a second order derivatives. To reduce the computation error

and improve numerical instability, we separately search for the descent direction of  $\mu_1$  and  $\mu_2$  for the two energy terms  $\int_{S_1} (I_1 - I_2(f^\mu))^2$  and  $\int_{S_1} |\mu - \nu_n|^2$  respectively in the following way.

For the first term, we apply the Demon force proposed by Wang et al. [37] to find the deformation:

$$u = \frac{(I_1 - I_2)\nabla(I_2)}{|\nabla(I_2)|^2 + \alpha^2(I_1 - I_2)^2} + \frac{(I_1 - I_2)\nabla(I_1)}{|\nabla(I_1)|^2 + \alpha^2(I_1 - I_2)^2} \quad (5.22)$$

where  $u$  is the deformation vector field. The corresponding Beltrami coefficient of the deformation is

$$\mu_d = \frac{\partial(Id + u)}{\partial\bar{z}} / \frac{\partial(Id + u)}{\partial z} \quad (5.23)$$

By the composition rule of the Beltrami coefficient, we have

$$\mu(u(f)) = \frac{\mu(f) + \overline{\frac{f_z}{f_z}\mu_d}}{1 + \overline{\frac{f_z}{f_z}\mu(f)\mu_d}}, \quad (5.24)$$

where  $u(f) := (\mathbf{id} + u) \circ f$ . Then the descent direction  $d\mu_1$ , which minimizes  $\int_{S_1} (I_1 - I_2(f^\mu))^2$ , can be approximated by

$$d\mu_1 \approx \mu(u(f)) - \mu(f) \quad (5.25)$$

For the second term, we can obtain the descent direction as  $d\mu_2 = -2(\mu - \nu_n)$ . Therefore, the descent direction to solve the optimization problem is given by:

$$d\mu = \beta d\mu_1 + \sigma d\mu_2 \quad (5.26)$$

Using the Demon force as registration guarantee the smoothness of  $\mu_d$  and also stabilizes the algorithm.

**5.4. Multiresolution scheme.** To reduce the computation cost of registering high-resolution images or high-quality surface meshes, we adopt a multiresolution scheme for the registration procedure. In the multiresolution scheme, we first coarsen both  $I_1$  and  $I_2$  by  $k$  layers, where  $I_j^0 = I_j$  and  $I_j^k$  is the coarsest images of  $I_j$  ( $j = 1, 2$ ). The registration process starts with registering  $I_1^k$  and  $I_2^k$ . Diffeomorphism  $f_k$  can then be obtained. To proceed to finer scale, we adopt a linear interpolation on  $f_k$  to obtain  $f_{k-1}$ , which serves as the initial map for the registration at the finer layer. We keep the process going until the registration at the finest (original resolution) layer is obtained. This multiresolution scheme significantly speed up the computational time.

**6. Experimental results.** We have test our proposed algorithms on synthetic data together with real medical data. In this section, experimental results are reported.

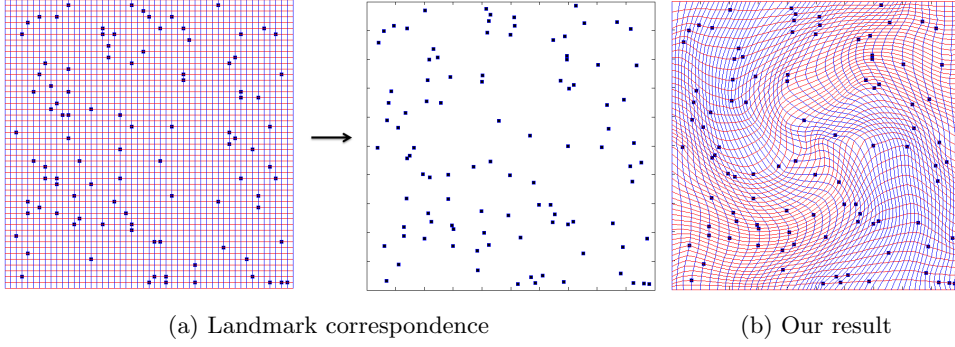


Fig. 6.1: Landmark-based registration with large amount of landmark constraints. (a) shows the correspondence between two landmark sets defined on two unit squares. (b) shows the obtained landmark-matching diffeomorphic registration using our proposed algorithm.

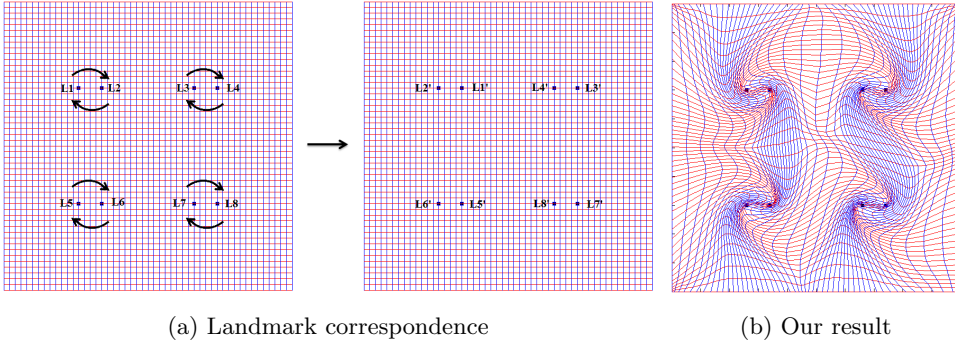


Fig. 6.2: Landmark-based registration with large deformations. (a) shows the correspondence between two landmark sets defined on two unit squares. (b) shows the obtained landmark matching diffeomorphic registration using our proposed algorithm.

### 6.1. Landmark-based registration.

*Example 1.* We first test our proposed landmark-based registration model on a synthetic example with large amount of landmark constraints enforced. Figure 6.1(a) shows the correspondence between two landmark sets defined on two rectangles. 78 corresponding landmark features are labeled on each rectangles. We compute the landmark matching diffeomorphic registration between the two rectangles, using our proposed landmark-based registration model. The registration result is as shown in (b), which is visualized by the deformation of the regular grids under the registration. Note that the obtained registration is bijective. No overlaps or flips can be found.

*Example 2.* In this example, we test our proposed algorithm on a synthetic example to obtain a landmark matching registration between two rectangles with very large deformations. Figure 6.2(a) shows two rectangles, with corresponding landmark sets defined on each of them. The prescribed deformations of the landmarks are large. Using our proposed landmark-based registration model, we compute the landmark matching diffeomorphic registration between the two rectangles. The registration re-

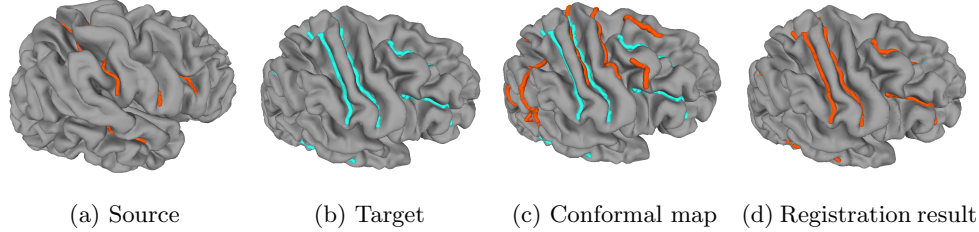


Fig. 6.3: (a) and (b) show two brain cortical surfaces, each of them is labeled with six corresponding sulcal landmarks. (c) shows the conformal registration between the two surfaces without landmark matching. (d) shows the registration result using our proposed landmark-matching quasi-conformal registration.

sult is as shown in (b), which is visualized by the deformation of the regular grids under the registration. Note that the obtained registration is bijective. No overlaps or flips can be found.

*Example 3.* (Brain landmark matching registration) We apply the proposed algorithm to compute landmark matching quasi-conformal registration between brain cortical surfaces. Figure 6.3(a) and (b) show two brain cortical surfaces, each of them is labeled by 6 sulcal landmarks. Using our proposed method, we compute the landmark-matching quasi-conformal registration between them. Figure 6.3(c) shows the conformal registration between the two surfaces. Note that the corresponding landmarks cannot be matched. Figure 6.3(d) shows the registration result using our proposed landmark-matching quasi-conformal registration, which matches corresponding landmarks consistently. Figure 6.4 (a) shows the energy plot versus iterations. It demonstrates our method iteratively minimizes the energy functional to an optimal quasi-conformal map between the two brain surfaces. (b) shows the maximum landmark error versus iterations. In Figure 6.5, we compute the landmark-matching quasi-conformal registrations with 6 sulcal landmarks between 10 brain cortical surfaces. The mean surface is then computed after the cortical surfaces are registered. The sulcal features are well-preserved, illustrating that the landmarks are consistently matched under the registration.

Table 6.1: Comparison with other methods with different sizes of deformation

(Time / Overlap)	Tiny	Moderate	Large
QC	6.220 s / 0	9.632 s / 0	12.934 s / 0
Harmonic Map	1.633 s / 13	1.665 s / 42	1.652 s / 110
TPS	0.308 s / 20	0.339 s / 27	0.253 s / 27
LDDMM	382.316 s / 0	396.240 s / 0	409.902 s / 0

*Example 4.* We also compared our proposed landmark-matching quasi-conformal registration algorithm with other state-of-the-art algorithms, namely, 1. harmonic map [38, 28, 26, 27]; 2. thin-plate spline (TPS) [1] and 3. LDDMM [22, 12, 13, 9, 10]. Experiments have been carried out for different sizes of deformations. As shown in Table 6.1, our method outperforms other methods. In all cases (tiny, moderate and large deformations), our method is able to compute a non-overlapping landmark-matching

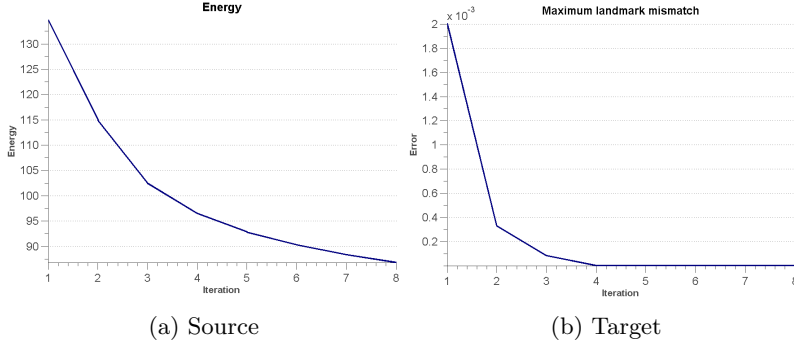


Fig. 6.4: (a) shows the energy plot versus iterations for the landmark-matching quasi-conformal registration between brain cortical surfaces. (b) shows the maximum landmark matching error versus iterations.

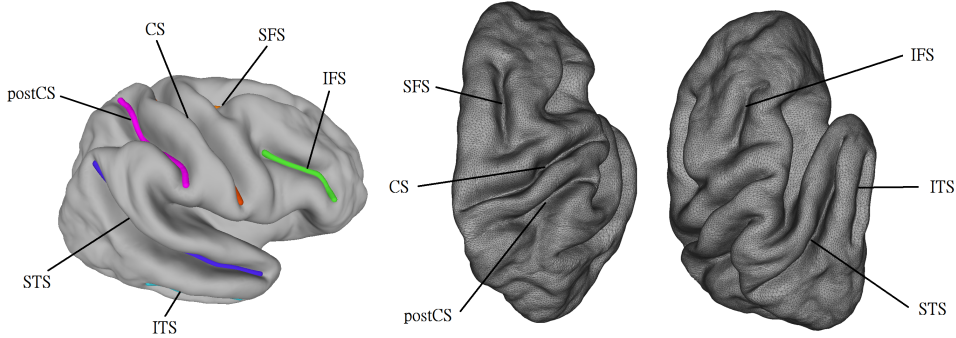


Fig. 6.5: Using the proposed algorithm, the landmark-matching quasi-conformal registrations with 6 sulcal landmarks between 10 brain cortical surfaces are obtained. The mean surface is then computed after the cortical surfaces are registered. The sulcal features are well-preserved, illustrating that the landmarks are consistently matched under the registration.

registration with the least amount of computational time. Both harmonic map and TPS has overlaps for their obtained registration results, although the computations of these methods are efficient. LDDMM can obtain non-overlapping landmark-matching registrations, however, the computational cost is comparatively much more expensive.

## 6.2. Q-Fibra Hybrid registration.

*Example 5.* We next test our proposed Q-Fibra hybrid registration algorithm on a synthetic example. Figure 6.6(a) and (b) shows two synthetic images to be registered. (a) shows the image of the character ‘A’. (b) shows the image of the character ‘R’. Corresponding feature landmarks are labeled on each images. Our goal is to look for a diffeomorphic registration that matches the corresponding landmarks and also the image intensities. (c) shows the obtained diffeomorphic registration using our proposed Q-Fibra hybrid registration model. Image 1 in (a) is deformed using the obtained registration to get a deformed image, which is shown in (c). The deformed image closely resembles to the target image (Image 2 in (b)). Landmarks

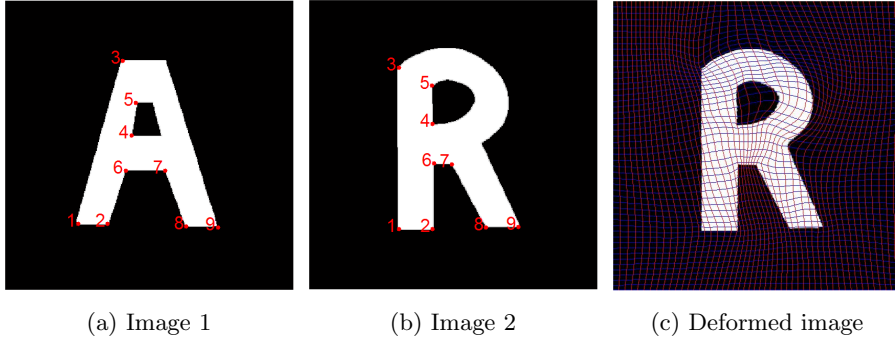


Fig. 6.6: (a) and (b) show two images to be registered. Corresponding feature landmarks are labeled on each images. (c) shows the obtained diffeomorphic registration using our proposed Q-Fibra hybrid registration model.

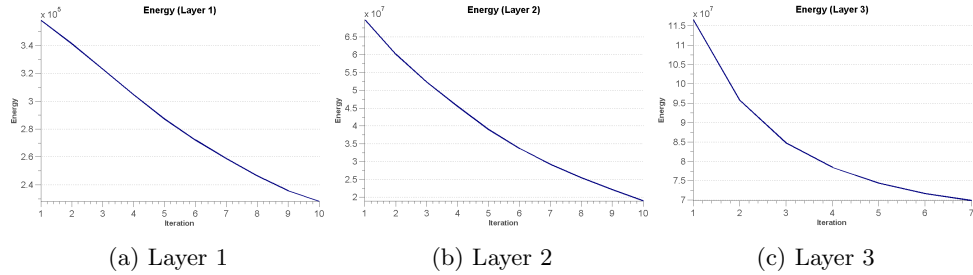


Fig. 6.7: The plots of energy versus iterations for the hybrid registration between the ‘A’ and ‘R’ images. Multiresolution scheme is applied to perform the registration from the coarsest layer to the finest (original resolution) layer. The energy plots at different layers are shown.

are consistently matched, and the obtained registration is bijective. Figure 6.7 shows the plots of energy versus iterations. In our algorithm, multi-resolution scheme is applied to perform the hybrid registration from the coarsest layer to the finest (original resolution) layer. In this example, three layers are used. Layer 1 refers to the coarsest resolution and layer 3 refers to the finest (original) resolution. The energy plots at different layers are shown in Figure 6.7. The energy is significantly reduced during the optimization process at the first layer. The obtained coarse registration is then interpolated back to the finer layer. An optimal solution is finally reached during the optimization process at the third layer using about 10 iterations. Figure 6.8 shows the optimal registration at different layers of the multiresolution scheme.

*Example 6.* We also test the proposed Q-Fibra hybrid registration algorithm on another synthetic example with larger deformation. Figure 6.9(a) and (b) shows two synthetic images to be registered. (a) shows the image of the character ‘T’. (b) shows the image of the character ‘C’. Corresponding feature landmarks are labeled on each images. Again, the goal is to look for a diffeomorphic registration that matches the corresponding landmarks and also the image intensities. (c) shows the obtained diffeomorphic registration using our proposed Q-Fibra hybrid registration

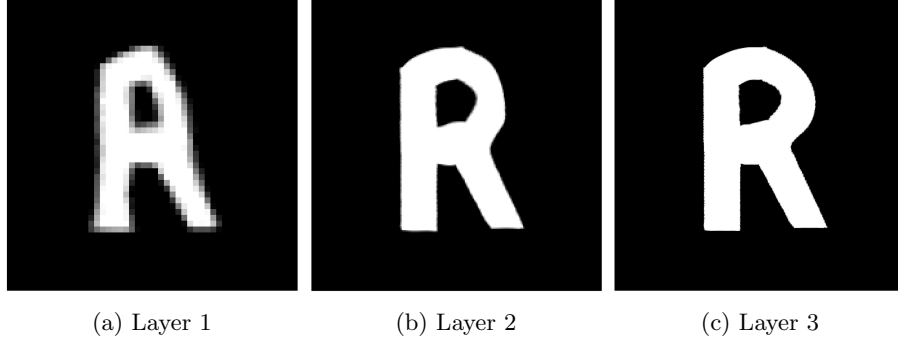


Fig. 6.8: The registration results using the multiresolution scheme with 3 layers.

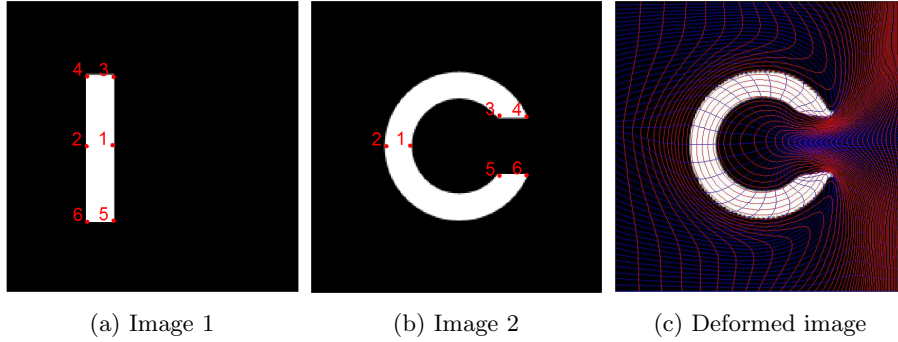


Fig. 6.9: (a) shows the image of the character ‘I’. (b) shows the image of the character ‘C’. These two images are to be registered. Corresponding feature landmarks are labeled on each images. (c) shows the obtained diffeomorphic registration using our proposed Q-Fibra hybrid registration model.

model. Image 1 in (a) is deformed using the obtained hybrid registration to get a deformed image, which is shown in (c). The deformed image closely resembles to the target image (Image 2 in (b)). Landmarks are consistently matched, and the obtained registration is bijective.

*Example 7.* We test the Q-Fibra hybrid registration algorithm on real images. Figure 6.10 shows two images of the human hands. Corresponding landmark features are labeled on each images. In Figure 6.11, we show the registration results using different approaches. Figure 6.11(b) shows the deformed image from Image 1 using our proposed landmark-based registration model. Notice that if we only use landmarks as constraints to guide the registration, the deformed image is very different (see regions in the red boxes) from the target image (as shown in (a)). (c) shows the deformed image from Image 1 using the intensity-based registration. Similarly, the deformed image is very different (see regions in the red boxes) from the target image if only intensity information is used. (d) shows the deformed image from Image 1 using the proposed Q-Fibra hybrid registration model. The deformed image closely resembles to the target image. In fact, the intensity mismatching error is about 1.32%, which is small, meaning that the registration is very accurate.

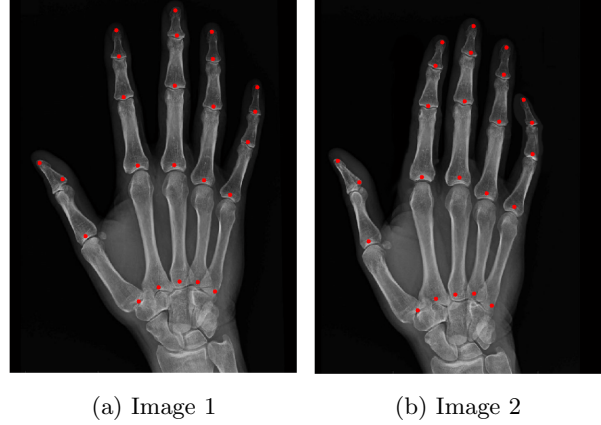


Fig. 6.10: Two images of human hands to be registered. Corresponding landmark features are labeled on each image.

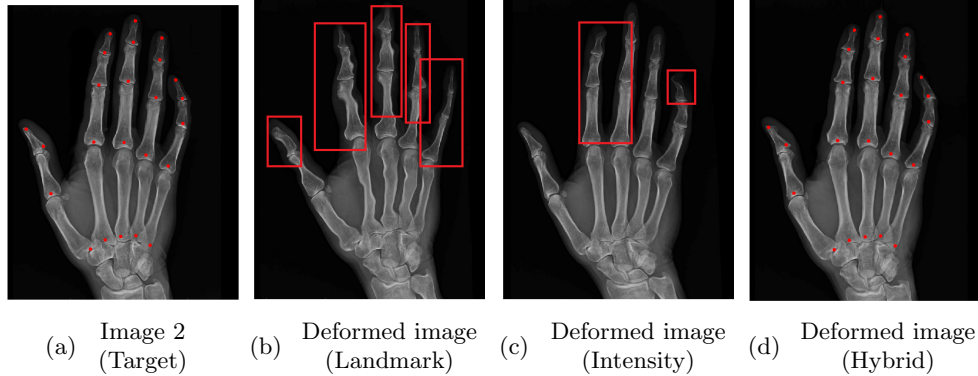


Fig. 6.11: Registration results of the human hand images using different approaches. (a) shows the target image (Image 2 as in Figure 6.10). (b) shows the deformed image from Image 1 using the landmark-based registration model. (c) shows the deformed image from Image 1 using the intensity-based registration model. (d) shows the deformed image from Image 1 using the proposed Q-Fibra hybrid registration model.

*Example 8.* We also test the Q-Fibra hybrid registration algorithm to register two brain MRIs. Figure 6.12 shows two human brain images. Corresponding landmark features are labeled on each images. In Figure 6.13, we show the registration results using different approaches. Figure 6.13(b) shows the deformed image from Image 1 using our proposed landmark-based registration model. If we only use landmarks as constraints to guide the registration, the deformed image is different (see regions in the red boxes) from the target image (as shown in (a)). (c) shows the deformed image from Image 1 using the intensity-based registration. Similarly, the deformed image is very different (see regions in the red boxes) from the target image if only intensity information is used. Notice that local minimum is reached using the intensity-based

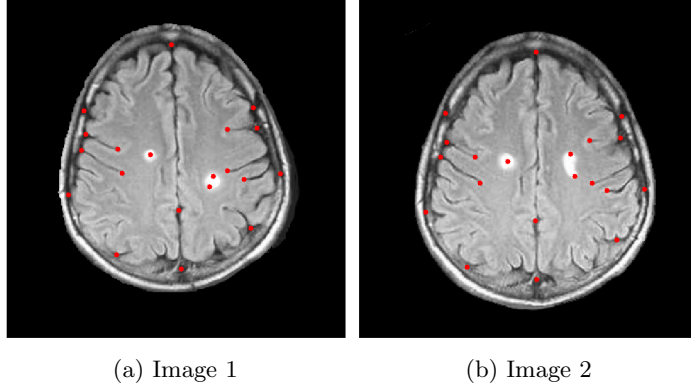


Fig. 6.12: Two human brain images to be registered. Corresponding landmark features are labeled on each images.

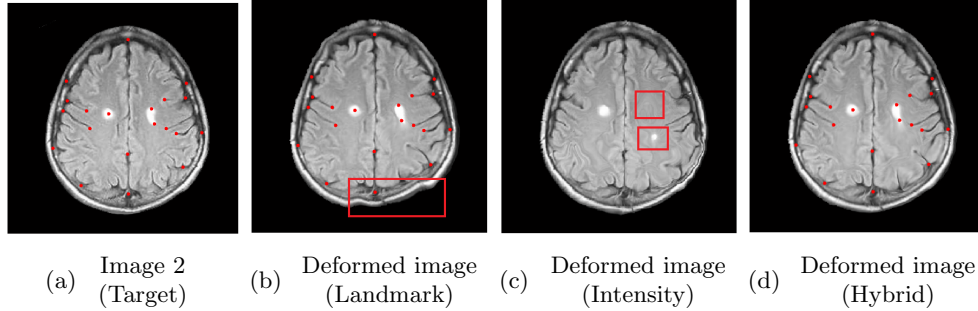


Fig. 6.13: Registration results of the human brain images using different approaches. (a) shows the target image (Image 2 as in Figure 6.12). (b) shows the deformed image from Image 1 using the landmark-based registration model. (c) shows the deformed image from Image 1 using the intensity-based registration model. (d) shows the deformed image from Image 1 using the proposed Q-Fibra hybrid registration model.

registration. (d) shows the deformed image from Image 1 using the proposed Q-Fibra hybrid registration model. The deformed image closely resembles to the target image. The intensity mismatching error is about 1.81%, which is small, meaning that the registration is very accurate.

*Example 9.* In this example, we compare our proposed Q-Fibra hybrid registration with other existing registration algorithms to register images with tiny, moderate and large deformations respectively. We compare our proposed method with TPS landmark-based registration [1], Demon intensity-based registration [34], and DROP hybrid registration (TPS landmark-matching + MRF intensity-matching registration) [6][7][5]. Table 6.2 shows the comparison with others to register images with tiny deformation. In the table,  $e_{\max}$  and  $e_{\text{mean}}$  are the maximal and average landmark mismatching error respectively. It is observed that landmarks cannot be matched consistently using TPS, Demon and DROP. Our method is able to match landmarks

Table 6.2: Comparison of the proposed hybrid registration with other methods (tiny deformation)

Method	$e_{\max}$	$e_{\text{mean}}$	Int. Diff. (%)	Flipping (%)
TPS	0.0706	0.0375	16.3759	0
Demon	0.1863	0.0875	1.7288	3.5955
DROP	0.0645	0.0407	1.6010	0.0208
Proposed	$2.698 \times 10^{-14}$	$1.742 \times 10^{-14}$	0.893	0

Table 6.3: Comparison of the proposed hybrid registration with other methods (moderate deformation)

Method	$e_{\max}$	$e_{\text{mean}}$	Int. Diff. (%)	Flipping (%)
TPS	0.1008	0.0402	7.5365	0
Demon	0.1411	0.0354	0.1950	2.5276
DROP	0.1059	0.0408	2.5561	0.2004
Proposed	$3.165 \times 10^{-14}$	$2.014 \times 10^{-14}$	0.2743	0

Table 6.4: Comparison of the proposed hybrid registration with other methods (large deformation)

Method	$e_{\max}$	$e_{\text{mean}}$	Int. Diff. (%)	Flipping (%)
TPS	0.3176	0.1996	10.3934	93.3992
Demon	0.8504	0.5592	7.3914	0
DROP	0.2903	0.1772	9.1277	2.9254
Proposed	$1.463 \times 10^{-13}$	$6.314 \times 10^{-14}$	0.6767	0

consistently. The percentages of the intensity difference after the registration are also shown in the table. Our proposed Q-Fibra hybrid registration gives the minimal percentage of the intensity difference. Also, our method generates a registration without flippings (bijective) whereas both Demon and DROP produce registrations with flippings. Table 6.3 and 6.4 show the comparison to register images with moderate and large deformations respectively. Again, our proposed method can give registrations without flipping, which can match landmarks consistently and effectively match the image intensities. Note that in Table 6.4, the Demon algorithm stopped at the local minimum. Although the obtained registration has no flipping, the percentage of the intensity difference is relatively large.

*Example 10.* We also test the Q-Fibra hybrid registration algorithm to register two human teeth surfaces. Figure 6.14 shows two human teeth surfaces, each of them are labeled with corresponding landmarks. Figure 6.15 shows the registration results of the two teeth surfaces using the landmark-matching quasi-conformal registration. (a) shows the surface of Teeth 1, whose colormap is given by its mean curvature. (b) shows the surface of Teeth 2, whose colormap is given by its mean curvature. (c) shows the registration result using the landmark-matching quasi-conformal registration. The colormap on the surface of Teeth 1 is mapped to the surface of Teeth 2 using the

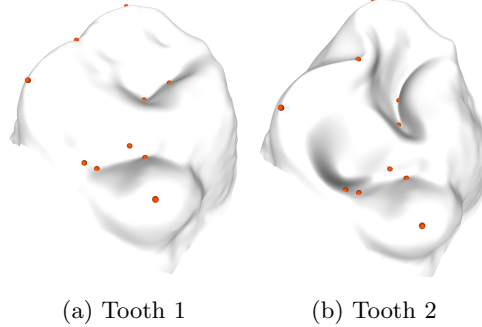


Fig. 6.14: Two human teeth to be registered, each of them are labeled with corresponding landmarks.

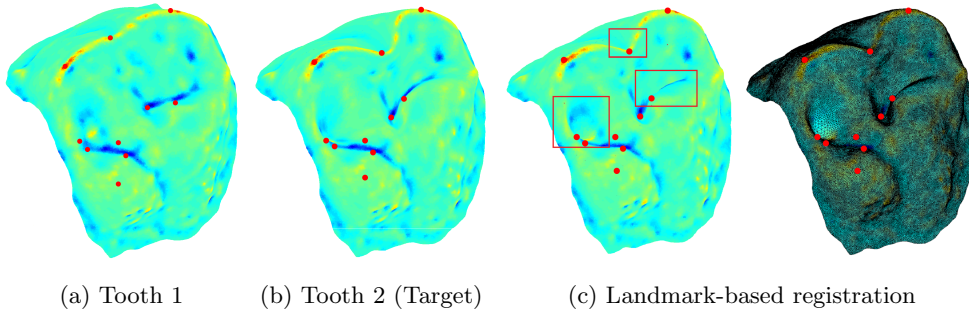


Fig. 6.15: Registration results of the two teeth surfaces using the landmark-matching quasi-conformal registration. (a) shows the surface of Teeth 1, whose colormap is given by its mean curvature. (b) shows the surface of Teeth 2, whose colormap is given by its mean curvature. (c) shows the registration result using the landmark-matching quasi-conformal registration. The colormap on the surface of Teeth 1 is mapped to the surface of Teeth 2 using the obtained registration. Note that the curvature is not matched consistently (see the regions in the red boxes).

obtained registration. Note that the curvature is not matched consistently (see the regions in the red boxes). It means the registration is not accurate if only landmark constraints are used to guide the registration process. Figure 6.16 (c) shows the registration result using the proposed Q-Fibra hybrid registration. In this case, both landmarks and curvature information are used to guide the registration process. The colormap (mean curvature) on the surface of Teeth 1 is mapped to the surface of Teeth 2 using the obtained registration. Note that the curvature is consistently matched, which means the registration result is accurate.

*Example 11.* We also test the Q-Fibra hybrid registration algorithm to register two human face surfaces. Figure 7.1 shows two human face surfaces, each of them are labeled with corresponding landmarks. Figure 7.2 shows the registration results of the two human faces using the proposed Q-Fibra hybrid registration. (a) shows the surface of human face 1, whose colormap is given by its mean curvature. (b) shows the surface of human face 2, whose colormap is given by its mean curvature. (c) shows

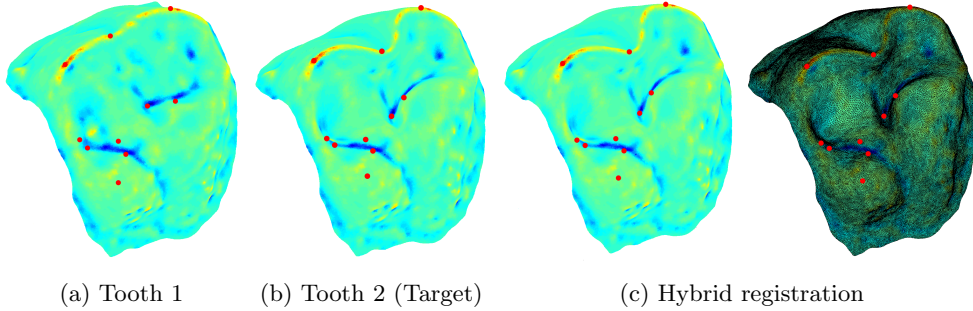
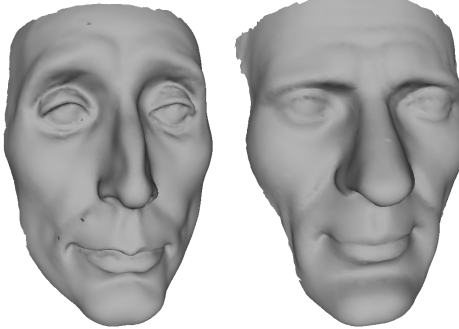


Fig. 6.16: Registration results of the two teeth surfaces using the hybrid quasi-conformal registration. (a) shows the surface of Teeth 1, whose colormap is given by its mean curvature. (b) shows the surface of Teeth 2, whose colormap is given by its mean curvature. (c) shows the registration result using the hybrid quasi-conformal registration. The colormap on the surface of Teeth 1 is mapped to the surface of Teeth 2 using the obtained registration. Note that the curvature is matched consistently.

the registration result using the proposed hybrid quasi-conformal registration. The colormap on the surface of human face 1 is mapped to the surface of human face 2 using the obtained registration. Note that the corresponding regions are consistently matched. (d) shows the plot of curvature mismatching energy versus iterations. It shows that our algorithm iteratively adjusts the quasi-conformal registration to an optimal one that minimizes the curvature mismatching error.

**7. Conclusion.** This paper presents a novel method to obtain diffeomorphic image or surface registrations with large deformations via quasi-conformal maps. The main strategy is to minimize an energy functional involving a Beltrami coefficient term. The Beltrami coefficient measures the conformality distortion of the quasi-conformal map. It controls the bijectivity and smoothness of the registration. By minimizing the energy functional, we obtain an optimal Beltrami coefficient associated to the desired registration, which is bijective, even with very large deformations. The proposed method can be applied for both landmark-based registration and hybrid registration (called *Q-Fibra*). Experiments have been carried out on both synthetic and real data. Results show that our proposed method can effectively obtain a smooth registration between images or surfaces with least amount of local geometric distortion. The obtained registration is also bijective (1-1 and onto), even with a large deformation or large number of landmark constraints. In the future, we plan to extend the proposed method to high-genus surfaces and apply the method to more real applications in medical imaging for disease analysis.



(a) Face 1 (b) Face 2

Fig. 7.1: Two human faces to be registered, each of them are labeled with corresponding landmarks. The mesh data are freely available at <http://shapes.aimatsshape.net>.

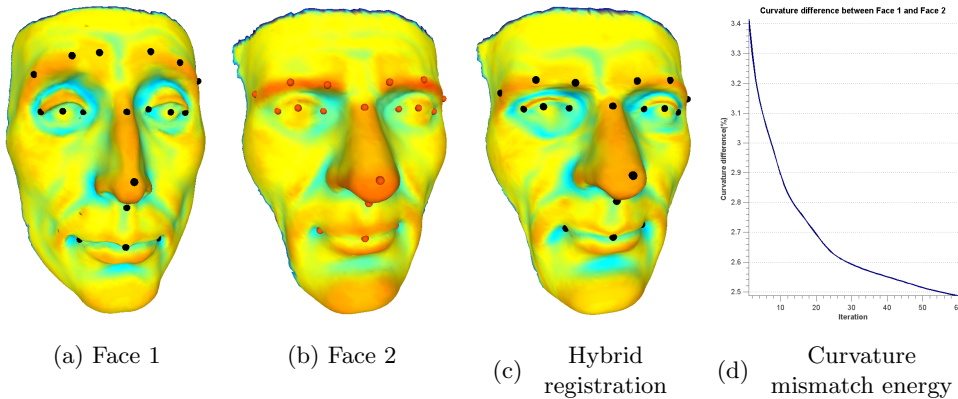


Fig. 7.2: Registration results of the two human faces using the hybrid quasi-conformal registration. (a) shows the surface of human face 1, whose colormap is given by its mean curvature. (b) shows the surface of human face 2, whose colormap is given by its mean curvature. (c) shows the registration result using the hybrid quasi-conformal registration. The colormap on the surface of human face 1 is mapped to the surface of human face 2 using the obtained registration. Note that the corresponding regions are consistently matched. (d) shows the plot of curvature mismatching energy versus iterations.

**Acknowledgment.** Lok Ming Lui is supported by RGC GRF (Project ID: 401811).

## REFERENCES

- [1] F. L. Bookstein. Principal Warps: Thin-Plate splines and the decomposition of deformations. *IEEE Transactions on Pattern Analysis and Machine Intelligence*, 11(6), 567–585, 1989.
- [2] T. Chanwimaluang and G. Fan. Hybrid retinal image registration. *IEEE Transaction on Information Technology in Biomedicine*, 10(1), 129–142, 2006.
- [3] B. Fischl, M. Sereno, R. Tootell, and A. Dale. High-resolution intersubject averaging and a coordinate system for the cortical surface. *Human Brain Mapping*, 8, 272–284, 1999.
- [4] F. Gardiner and N. Lakic. *Quasiconformal Teichmuller Theory*. American Mathematics Society, 2000.
- [5] B. Glocker and N. Komodakis. DROP: Deformable image registration using discrete optimization. Software available at: <http://www.mrf-registration.net/>.
- [6] B. Glocker, N. Komodakis, N. Paragios and N. Navab. Approximated curvature penalty in non-rigid registration using pairwise mrfs. *5th International Symposium on Visual Computing (ISVC)*, Las Vegas, Nevada, USA, November 2009.
- [7] B. Glocker, N. Komodakis, N. Paragios, G. Tziritas, and N. Navab. Inter and intra-modal deformable registration: Continuous deformations meet efficient optimal linear programming. *Information Processing in Medical Imaging*, Kerkrade, Netherlands, July 2007.
- [8] B. Glocker, N. Komodakis, G. Tziritas, N. Navab, and N. Paragios Dense image registration through mrfs and efficient linear programming. *Medical Image Analysis*, 12(6):731–741, 2008.
- [9] J. Glaunes, A. Qiu, M. Miller and L. Younes. *Large Deformation Diffeomorphic Metric Curve Mapping*, International Journal of Computer vision, 80(3), 317–336, 2008.
- [10] J. Glaunes, A. Qiu, M. Miller and L. Younes. *Surface Matching via Currents*. Proceedings of Information Processing in Medical Imaging (IPMI'05), Vol. 3565, 381–392, 2005.
- [11] B. Glocker, A. Sotiras, N. Komodakis and N. Paragios. Deformable Medical Image Registration: Setting the State of the Art with Discrete Methods. *Annual Review of Biomedical Engineering*, 12(12), 219–244, 2011.
- [12] J. Glaunès, M. Vaillant and M. I. Miller. Landmark Matching via Large Deformation Diffeomorphisms on the Sphere. *Journal of Mathematical Imaging and Vision*, 20, 179–200, 2004.
- [13] J. Glaunes, L. Younes and A. Trouve. Diffeomorphic matching of distributions: A new approach for unlabelled point-sets and sub-manifolds matching, *IEEE Computer Society Conference on Computer Vision and Pattern Recognition (CVPR'04)*, 2, 712–718, 2004.
- [14] X. F. Gu, Y. Wang, T. F. Chan, P. M. Thompson, and S.-T. Yau. Genus zero surface conformal mapping and its application to brain surface mapping. *IEEE Transactions on Medical Imaging*, 23(8), 949–958, 2004.
- [15] X. F. Gu and S. Yau. Computing conformal structures of surfaces. *Communication in Information System*, 2(2), 121–146, 2002.
- [16] S. Haker, S. Angenent, A. Tannenbaum, R. Kikinis, G. Sapiro, and M. Halle. Conformal surface parameterization for texture mapping. *IEEE Transaction of Visualization and Computer Graphics*, 6, 181–189, 2000.
- [17] X. Huang, Y. Sun, D. Metaxas, F. Sauer and C. Xu. Hybrid Image Registration based on Configural Matching of Scale-Invariant Salient Region Features. *Proceedings of the 2004 Conference on Computer Vision and Pattern Recognition Workshop (CVPRW'04)*, Volume 11, 167–174, 2004.
- [18] M. K. Hurdal and K. Stephenson. Discrete conformal methods for cortical brain flattening, *Neuroimage*, 45, 86–98, 2009.
- [19] A. Jacobson, O. Sorkine. A Cotangent Laplacian for Images as Surfaces. *ACM Trans. Graph*, 25(3), 646–653, 2012.
- [20] M. Jin, J. Kim, F. Luo and X. F. Gu. Discrete surface Ricci flow. *IEEE Transaction on Visualization and Computer Graphics*, 14(5), 1030–1043, 2008.
- [21] H. J. Johnson and G. E. Christensen. Consistent landmark and intensity-based image registration. *IEEE Transactions on Medical Imaging*, 21, 450–461, 2002.
- [22] S. Joshi and M. Miller. Landmark matching via large deformation diffeomorphisms. *IEEE Transactions on Image Processing*, 9(8), 1357–1370, 2000.
- [23] O. Lehto and K. Virtanen. *Quasiconformal Mappings in the Plane*. Springer-Verlag, New York, 1973.
- [24] T. Lin, C. L. Guyader, I. Dinov, P. Thompson, A. Toga, L. Vese. Gene Expression Data to Mouse Atlas Registration Using a Nonlinear Elasticity Smoother and Landmark Points Constraints. *Journal of Scientific Computing*, 50(3), 586–609, 2012.
- [25] N. A. Lord, J. Ho, B. C. Vemuri and S. Eisenschenk. Simultaneous Registration and Parcel-

- lation of Bilateral Hippocampal Surface Pairs for Local Asymmetry Quantification. *IEEE Transactions on Medical Imaging*, 26(4), 471-478, 2007.
- [26] L. M. Lui, S. Thiruvenkadam, Y. Wang, T. Chan, and P. Thompson. Optimized conformal parameterization of cortical surfaces using shape based matching of landmark curves. *Proceeding in Medical Image Computing and Computer-Assisted Internvention - MICCAI 2005*, 494–502, 2008.
- [27] L. M. Lui, S. Thiruvenkadam, Y. Wang, P. Thompson, and T. Chan. Optimized conformal surface registration with shape-based landmark matching. *SIAM Journal of Imaging Sciences*, 3(1), 52–78, 2010.
- [28] L. M. Lui, Y. Wang, T. Chan, and P. Thompson. Landmark constrained genus zero surface conformal mapping and its application to brain mapping research. *Applied Numerical Mathematics*, 57, 847–858, 2007.
- [29] L. M. Lui, T. W. Wong, W. Zeng, X. F. Gu, P. M. Thompson, T. F. Chan and S. T. Yau. Optimization of Surface Registrations Using Beltrami Holomorphic Flow. *Journal of Scientific Computing*, 50(3), 557–585, 2012.
- [30] L. M. Lui, T. W. Wong, X. F. Gu, P. M. Thompson, T. F. Chan and S. T. Yau. Hippocampal Shape Registration using Beltrami Holomorphic flow. *Medical Image Computing and Computer Assisted Intervention(MICCAI)*, Part II, LNCS 6362, 323–330 (2010).
- [31] L. M. Lui, K. C. Lam, T. W. Wong, X. F. Gu. Texture Map and Video Compression Using Beltrami Representation. *SIAM Journal on Imaging Science*, 6(4), 1880–1902, 2013.
- [32] O. Lyttelton, M. Boucher, S. Robbins, and A. Evans. An unbiased iterative group registration template for cortical surface analysis. *NeuroImage*, Vol 34, 1535–1544, 2007.
- [33] D. Paquin, D. Levy and L. Xing. Hybrid multiscale landmark and deformable image registration. *Math Biosci Eng.*, 4(4), 711–737, 2007.
- [34] J. P. Thirion. Image matching as a diffusion process an analogy with Maxwell’s demons. *Medical Image Analysis*, Vol 15, 112–115, 1996.
- [35] D. Tosun, M. Rettmann and J. Prince. Mapping techniques for aligning sulci across multiple brains. *Medical Image Analysis*, 8, 295–309, 2004.
- [36] T. Vercauteren, X. Pennec, A. Perchant and N. Ayache. Diffeomorphic demons: Efficient non-parametric image registration. *NeuroImage*, 45(1), S61S72, 2009.
- [37] H. Wang, L. Dong, J. O’Daniel, R. Mohan, A. S. Garden, K. K. Ang, and R. Cheung. Validation of an accelerated ‘demons’ algorithm for deformable image registration in radiation therapy. *Physics in Medicine and Biology*, 50(12): 2887, 2005.
- [38] Y. Wang, L. M. Lui, T. Chan, and P. Thompson. Optimization of brain conformal mapping with landmarks. *Proceeding in Medical Image Computing and Computer-Assisted Internvention - MICCAI 2005*, 675–683, 2005.
- [39] Y. Wang, L. M. Lui, X. F. Gu, K. M. Hayashi, T. F. Chan, A. W. Toga, P. M. Thompson, and S.-T. Yau. Brain surface conformal parameterization using riemann surface structure. *IEEE Transactions on Medical Imaging*, 26(6), 853–865, 2007.
- [40] Y. L. Yang, J. Kim, F. Luo, S. Hu, X. F. Gu. Optimal Surface Parameterization Using Inverse Curvature Map. *IEEE Transactions on Visualization and Computer Graphics* , 14(5), 1054–1066, 2008.
- [41] B. T. Yeo, M. R. Sabuncu, T. Vercauteren, N. Ayache, B. Fischl, P. Golland. Spherical demons: fast diffeomorphic landmark-free surface registration. *IEEE Transactions on Medical Imaging*, 29(3), 650668, 2010.
- [42] W. Zeng and X. F. Gu. Registration for 3D Surfaces with Large Deformations Using Quasi-Conformal Curvature Flow. *IEEE Conference on Computer Vision and Pattern Recognition (CVPR11)*, Jun 20-25, 2011, Colorado Springs, Colorado, USA.
- [43] W. Zeng, L. M. Lui, F. Luo, T. F. Chan, S. T. Yau, X. F. Gu. Computing quasiconformal maps using an auxiliary metric and discrete curvature flow. *Numerische Mathematik*, 121(4), 671–703, 2012.
- [44] W. Zeng, L. M. Lui, L. Shi, D. Wang, W. C. Chu, J. C. Cheng, J. Hua, S. T. Yau, X. F. Gu. Shape Analysis of Vestibular Systems in Adolescent Idiopathic Scoliosis Using Geodesic Spectra. *Medica Image Computing and Computer Assisted Internvention*, 13(3), 538–546, 2010.
- [45] B. Zitova and J. Flusser. Image registration methods: a survey. *Image and Vision Computing*, Volume 21, 977–1000, 2003